Planar Artificial Magnetic Conductors and Patch Antennas

Ying Zhang, *Student Member, IEEE*, Jürgen von Hagen, *Senior Member, IEEE*, Marwan Younis, *Student Member, IEEE*, Christian Fischer, *Student Member, IEEE*, and Werner Wiesbeck, *Fellow, IEEE*

***Abstract*—Surfaces act as perfect magnetic conductors (PMC) if the phase shift of the reflection of an electromagnetic wave amounts to 180° compared to the reflection at a perfect electric conductor (PEC). One possibility to create PMC surfaces artificially is an array of closely spaced patches. In this paper, based on the relation between PMC surfaces and patch antennas, an explanation for the functioning of this artificial PMC is given. An equivalent network is derived that allows to understand the functioning and to provide a starting design for a numerical optimization by aid of fullwave methods. A planar PMC is used for the first time as a reflector for a large aperture coupled patch antenna array, especially in order to reduce the parallel-plate modes that are usually present in traditional aperture coupled patch arrays. An additional sidelobe suppression of over 6 dB has been achieved by the planar PMC reflector in comparison to a traditional reflector.**

***Index Terms*—Aperture coupled patch array, parallel-plate mode, patch antenna, perfect electric conductor (PEC), perfect magnetic conductors (PMC), reflection coefficient, sidelobe suppression.**

I. Introduction

THE reflection coefficient of a plane TEM wave incidence on a perfect electric conductor (PEC) is $\Gamma = -1$. The electromagnetically dual surface to a PEC surface is a perfect magnetic conductor (PMC); it exhibits a reflection coefficient of $\Gamma = +1$, which means that the phase of the reflected wave is 0° compared to the phase of the incident wave. In analogy to the theory of lines, these two reflecting surfaces could be called "short circuit" and "open circuit" where the latter is nonradiating. However, so far no physical PMC surfaces have been found that operate over a wide frequency band.

Reversely, a surface that shows a 180° phase shift compared to a PEC surface and, at the same time, completely reflects an incident plane wave effectively acts as a PMC surface. Any surface that physically is not a PMC, but exhibits the same scattering properties, is then called an artificial PMC.

PMC surfaces show interesting properties. First, the image currents for PMCs are in-phase with the original current. This allows to utilize PMCs as reflectors in antennas and to place radiating elements very close to the PMC, which results in low profile antennas. Second, PMCs provide high-impedance surface conditions and, hence, suppress surface waves. This way the interference of surface waves with the main radiation, and the associated edge effects can be reduced. To date, planar artificial PMC surfaces are receiving more and more attention in antenna applications since they offer advantages that cannot be accomplished by utilizing traditional PEC reflectors. Hence, the analysis and design of a PMC is important, especially for shrinking the size of antennas.

One possibility to design an artificial PMC is to use periodic structures. High-impedance electromagnetic surfaces have been studied by Sievenpiper [1]. In his approach, high-impedance surfaces consist in general of a lattice of metal plates, connected to a solid metal sheet by vertical conducting vias. However, vias are difficult and expensive to fabricate. To overcome this shortcoming, other planar structures [2], [3] have been proposed that do not incorporate vias. These alternative surfaces are composed of patches, one or more host substrates and ground planes. At a first look, these various proposed structures seem to be different from each other. A careful examination however reveals, that they have a common point: the basic element is a patch, either square or rectangular. The different sized and shaped patches are repetitively positioned at a certain period, forming the different structures.

The purpose of this paper is twofold: first, to provide further knowledge on the functioning of artificial PMCs, and second, to present the practical application of an artificial PMC to a large aperture coupled patch antenna array as a reflector. The aim is to reduce the parallel-plate modes that propagate between the plane with the coupling apertures and the backside reflector.

To understand the performance of various planar PMC structures, it is suitable to investigate as a test structure a simple patch array hosted on a substrate with a ground plane. In Section II, the field distribution on a patch array is computed for a plane wave normally incident with a finite-difference time-domain (FDTD) method. Founded on the insight into the field distribution, a transmission-line model is then derived that helps the understanding of the functioning and the starting of the design phase for developing PMC surfaces. Further, the functioning of this planar PMC is explained with the behavior of a patch antenna. In Section III, this planar PMC is applied as a reflector to a 64-element aperture coupled patch antenna array.

II. Functioning of Planar PMC

Here, we explore the basic principles of artificial PMCs, using a simple patch array on a substrate backed by a ground plane as an example. The investigated artificial PMC has the following dimensions:

- The structure consists of square patches with an edge length of $W = L = 9.5\ \mathrm{mm}$.

Manuscript received September 27, 2002; revised December 3, 2002.

The authors are with the Institut für Höchstfrequenztechnik und Elektronik (IHE), Universität Karlsruhe (TH), D-76128 Karlsruhe, Germany (e-mail: ihe@ihe.uka.de).

Digital Object Identifier 10.1109/TAP.2003.817550

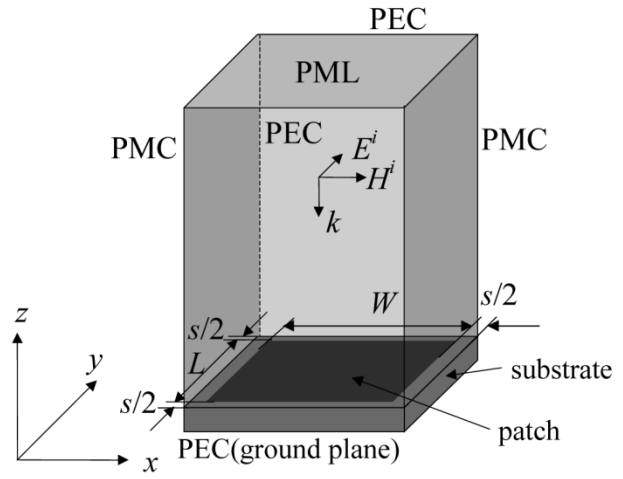

Fig. 1. FDTD model for an infinite patch array surface.

- The patches are situated on a homogeneous epoxy substrate with a permittivity of $\varepsilon_{\rm r} = 3.5$ and a thickness $h_{\rm subs} = 1.57\,{\rm mm}$.
- In the periodic structure, the patches have a separation of $s = 0.5\,{\rm mm}$. The resulting period of the structure is, hence, $P = 10\,{\rm mm}$.

In order to compute the structure, an FDTD method is employed. For the modeling, it is unnecessary to simulate an infinite structure. By the application of mirror boundary conditions around the single patch, the model of a single element can be used to simulate an infinite structure. A similar approach is used in [4]. Fig. 1 shows the FDTD model. Due to a geometrical and electrical symmetry of each single element, the sidewalls can be replaced by appropriate boundary conditions. This results in a correct modeling of an infinite structure considering only one single element, as the boundary conditions correctly reproduce the effects of all other elements. The incident electric field is polarized in the y direction, hence, the boundaries $y = y_{\rm min}$ and $y = y_{\rm max}$ are set to PEC so that the E-vector is normal to the boundary. $x_{\rm min}$ and $x_{\rm max}$ are set to PMC so that the magnetic field is normal to the boundary. $z_{\rm min}$ is set to PEC due to the ground plane. The wave is incident from $z = +\infty$ direction, the reflected wave is propagating in $+z$ direction and should be propagating with no reflection at the borders of the computational domain. Hence, $z_{\rm max}$ is set to perfectly matched layer (PML) to rule out an interference caused by the reflected wave at a distance of $z_{\rm comput} = 8\,{\rm mm}$. The computational domain is limited by the patch size plus an $s/2$ wide strip around the patch at the two sides, in this case, $x_{\rm comput} = y_{\rm comput} = s/2 + L + s/2 = 10\,{\rm mm}$, see Fig. 1.

The determination of the reflection properties of the periodic structure is a two-step process. In a first step, the reflection properties are computed over a wide frequency band in order to detect resonant frequencies. In a second step, the reflection coefficient at each resonant frequency is computed in magnitude and phase.

In the first step, the waveform of the incident wave should excite as many frequencies as possible, which is done using a raised-cosine pulse excitation. To extract the resonant frequencies at which the patch array acts as PMC, Prony's method [5] is applied. This method allows to obtain the exact resonant frequency. For the above defined structure, the simulated resonant frequency is $f_c = 5.45\,{\rm GHz}$. At this frequency, a further calculation is performed in the second step with a sine wave excitation. Comparing the incident and the reflected wave results in the reflection phase information. Measurements demonstrated a good agreement to simulations [6].

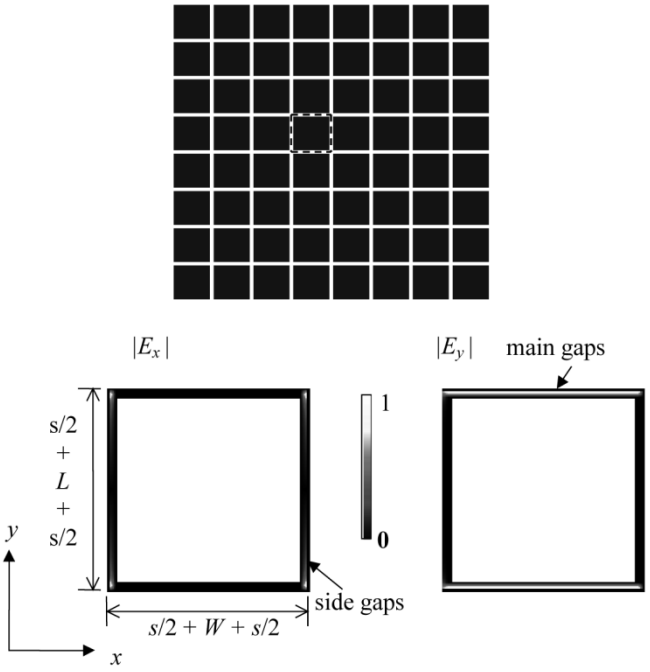

Fig. 2. Normalized field distribution of a patch array surface excited by a y-polarized normal TEM incident wave. Top is the patch array with the dashed line showing a single element taken as modeling element during the simulations. Bottom left are x-directed fields of an enlarged element; bottom right are y-directed fields. The big white surface is the surface of a single patch element of the top figure (zero field). The field is zero everywhere except in the small slot regions.

In the following, the field distribution is computed, which leads to the equivalent circuit model. The equivalent model in combination with the functioning of a square patch antenna explains the operation principles of the artificial PMC.

A. Field Distribution

With the sine wave excitation at resonance, the field distribution of the patch array under a normally incident plane wave is computed and shown in Fig. 2. The tangential fields $E_{\rm x}$ and $E_{\rm y}$ are normalized to their maximum values $\mid E_{\rm x,max} \mid$ and $|E_{\rm y,max}|$, respectively. The field on the patch is zero as expected for a PEC. The leading and trailing edge of the patch ($y = y_{\rm min}$ and $y = y_{\rm max}$) show very high field values with a uniform distribution. At the side edges ($x = x_{\rm min}$ and $x = x_{\rm max}$), the field shows a typical cosine distribution, with a zero in the middle of the edge.

The field distribution in this patch array is very similar to the fields of a single patch antenna [7]. The field is mainly polarized in the direction of the incident wave and exhibits a resonance phenomenon. Based on the equivalent circuit model of a single patch antenna, the following section derives an equivalent circuit model for the array.

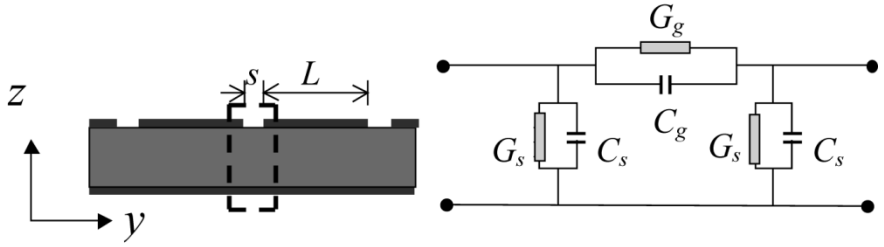

Fig. 3. Gap discontinuity and its π-network.

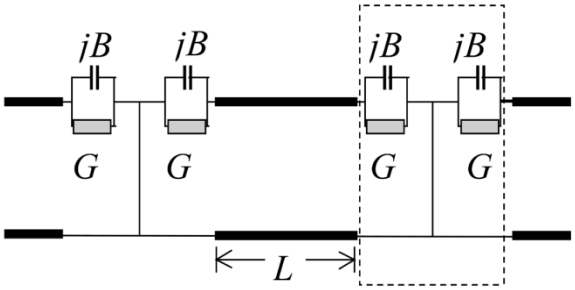

Fig. 4. Transmission line network (equivalent T-network is within the dotted rectangle).

B. Transmission-Line Model

According to [8], the equivalent circuit model of a single patch antenna consists of two parallel RC circuits representing the slot conductance and the radiation resistance that are connected by a transmission line representing the patch metallization.

Based on the previously computed field distribution and the assumed PEC boundaries at $y = y_{\min}$ and $y = y_{\max}$, the major contribution to the overall capacity in this resonant structure comes from the gap discontinuity at both ends of the patch. The patch itself with the current flow produces an inductance. The gap discontinuity is modeled as an odd-mode discontinuity [9] as is shown in Fig. 3: the capacity between the patch and the ground plane is C_s, the conductance accounting for radiation is G_s, the interpatch capacity at the main gaps of two patches is C_g and G_g is an additional conductance for losses and radiation. The π-network for the gaps is changed to a T-network for an easy treatment. The conversion from π to T is possible as the boundary conditions in the middle of the gap is a PEC or short circuit to ground: the electric field is normal to a surface normal to the ground plane in the middle of the gap. The admittances G_g and C_g are divided into two series elements with value $2G_g$ and $2C_g$ which are parallel to the slot impedances G_s and C_s. The final network is shown in Fig. 4 within the dotted rectangle. The admittances B and G are given by [9]

$$B = \omega C^o_{\rm eq} = \omega(C_s + 2C_g) \tag{1}$$

$$G = G_s + 2G_g \tag{2}$$

where ω is the angular frequency. For a given substrate, $C^o_{\rm eq}$ is proportional to the patch width W. If the gap capacitance per meter is C_0 in F/m and the patch width is W in m, then $C^o_{\rm eq} = WC_0$, which inserted into (1) gives

$$B = \omega C^o_{\rm eq} = \omega W C_0. \tag{3}$$

The transmission-line model for the patch array is finally obtained in Fig. 4. The admittance of one element is

$$Y = G + jB + Y_c \frac{G + j(B + Y_c \tan\beta L)}{Y_c - B\tan\beta L + jG\tan\beta L} \tag{4}$$

where β is the propagation constant and L is the length of the transmission line, in this situation equal to the patch length. Y_c is the characteristic admittance of the transmission line, neglecting any influence of the side gaps. The element resonates, when the imaginary part of the admittance vanishes. This occurs when the patch length satisfies

$$\tan\beta L = \frac{2Y_c B}{G^2 + B^2 - Y_c^2}. \tag{5}$$

The values of the parameters in (5) are functions of the physical configuration, namely substrate permittivity, thickness, patch width, patch length, separation width, and frequency. The general analysis of microstrip line gap discontinuities is described in [10].

Unfortunately, in the literature reference values are available only for a fixed set of parameters [11]. Furthermore, results based on quasi-static analysis are valid, with sufficient accuracy, only up to frequencies of a few GHz. For a complete characterization of discontinuities, the frequency dependency of various parameters is often determined by the more rigorous full-wave analysis. Still, the transmission line model offers a simple way to create an initial design as a starting point for a numerical optimization using a full-wave method.

As an example, we first design a single patch resonating at the operating frequency of the intended PMC surface, here $f = 5.45$ GHz. For the chosen substrate of $h_{\rm subs} = 1.57$ mm and $\varepsilon_{\rm r} = 3.5$, the effective dielectric constant is $\varepsilon_{\rm r,eff} = 2.974$, the effective wave length is then $\lambda_{\rm eff} = 31.89$ mm. For a single patch antenna, the starting point for an optimization process would be a patch length half of the effective wavelength [12], hence, $L_{\rm design} = 15.95$ mm. For a single patch, the slot capacitance of a patch on a substrate with height h is given by [12]

$$C_s = \frac{\varepsilon_0}{2}\left(1 - 0.636\ln(k_0 h)\right) \tag{6}$$

with the wavenumber k_0. According to (6) the slot capacitance amounts to $C_s = 9.27$ pF/m.

The equivalent capacitance of a microstrip-gap-discontinuity with a separation s and an odd field distribution is given by [9]

$$C^o_{\rm eq} = \frac{\varepsilon}{2\pi}\left[\ln 2 + \ln\left(\frac{A}{A-1} + \sqrt{\frac{A+1}{A-1}}\right)\right] \tag{7}$$

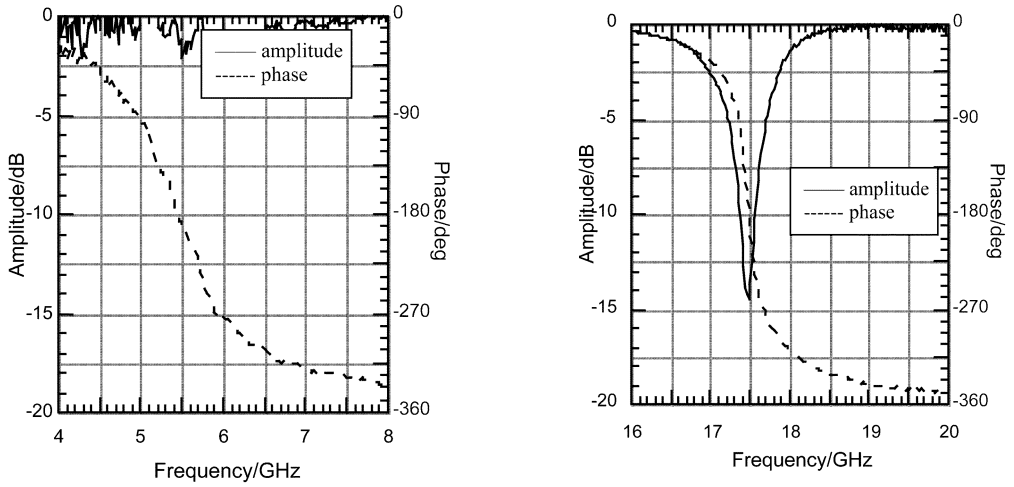

Fig. 5. Measured reflection coefficient of a PMC layer (amplitude:——— phase: – – – –).

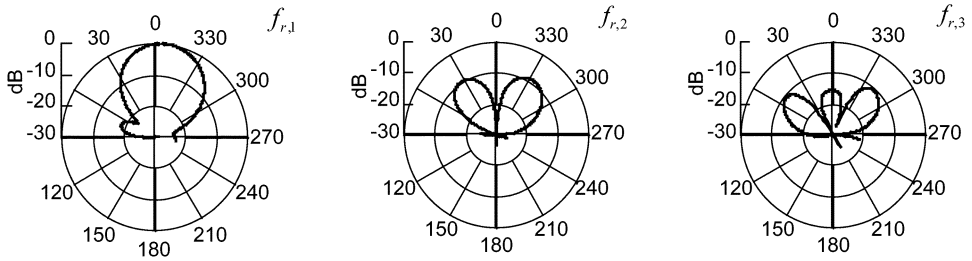

Fig. 6. Patterns of a single patch antenna.

with $A = \cosh(s\pi/2h)$. Strictly speaking, this capacitance is the static approximation of the electrodynamic capacitance, but it is used here within the validity range given in literature. For the chosen patch-to-patch separation of $s = 0.5\,\mathrm{mm}$, the equivalent capacitance (7) is $C^{o}_{\mathrm{eq}} = 16.03\ \mathrm{pF/m}$, hence a factor of 1.73 higher than that of the single patch. To account for the higher gap capacitance, the length of the patch should be shorter by this factor. The patch length in this case is then $L = 9.22\,\mathrm{mm}$ which is very close to the physical value of 9.5 mm.

To further verify the above transmission line model, the following two cases are calculated using the FDTD. The substrate permittivity, thickness, patch length, and gap width are fixed, values given at the begin of Section II, but the patch width is varied: 1) $W = 9.5\,\mathrm{mm}$; 2) $W = 4.75\,\mathrm{mm}$. The calculated resonant frequency in both cases is $f_c = 5.45\,\mathrm{GHz}$. That is to say, a modification of the patch width W with the patch length L remaining constant conserves the resonant frequencies of the patch array surface. The same result can be evolved from (5). In (5), G represents the radiation resistance, which is often much smaller than B or Y_c [8]. For example, for $0.1 \leq (W/\lambda_0) \leq 0.3$, the radiation resistance can be approximated by $G \approx 1/90\,(W/\lambda_0)^2$. This case is most often applicable to PMC surfaces. Therefore, G can be neglected. According to [12], if $W/h \gg 1$, where h is the height of the substrate, the characteristic admittance of a transmission line is

$$Y_c = \frac{\sqrt{\varepsilon_{\mathrm{reff}}}\left[\frac{W}{h} + 1.393 + 0.667\ln\left(\frac{W}{h} + 1.444\right)\right]}{120\pi} \approx \frac{\sqrt{\varepsilon_{\mathrm{reff}}}}{120\pi}\frac{W}{h}. \tag{8}$$

It can be seen that Y_c is quasi-proportional to the transmission line's width W, corresponding here to the width of the patch. B is also proportional to the patch width from (3). Thus, from (5), it can be seen that the resonant frequency mainly depends on the patch length L and is insensitive to the patch width W. This property of the PMC is similar to that of a patch antenna.

Other characteristics can be deduced from the transmission line model. For example, an enlargement of the gap width increases the resonant frequency; increasing the patch length decreases the resonant frequency; increasing the substrate permittivity decreases the resonant frequency; and an enlargement of the substrate thickness makes the resonant frequency decrease, etc. These characteristics have been verified by FDTD simulations.

C. Functioning of a Patch Array Surface

For experimental verification, an artificial PMC array of 20×20 square patch elements has been fabricated. The dimensions and physical properties are chosen in accordance to the above numerical model with its values given at the beginning of Section II.

The reflection properties of the specimen have been measured in an anechoic chamber. The specimen is illuminated by a wide band horn antenna whose gain is known over frequency. The reflected field is measured and normalized to the reflected field of a PEC surface previously mounted at exactly the same position as the specimen.

The patch array is now illuminated by a normal TEM wave with the electric field parallel to the plate and to one edge of

the patches. The reflection coefficient in amplitude and phase is measured and normalized to a PEC reflector. Thus, a 180° phase shift compared to a PEC reflector implies an in-phase reflection. From 4 to 20 GHz, two resonance phenomena are found. At the corresponding frequencies, the image current is in-phase compared to the original current as revealed by the phase curve Fig. 5(a) and (b).

The first resonant frequency is 5.45 GHz. The reflection coefficient is close to 0 dB [Fig. 5(a)], i.e., the complete power is reflected in specular direction. The second resonant frequency is at 17.5 GHz, a frequency about three times the first one. At this frequency the reflection coefficient exhibits a 14 dB deep dip [Fig. 5(b)]. No resonance at a frequency double of the first resonance is detected. For a high impedance surface, the power dip phenomenon of the reflected power for certain resonant frequency is also observed in [13].

As the constituent element of the array is a patch, the radiation characteristics of a single patch antenna are used for comparison. The radiation characteristics have been measured with a single patch antenna in the same anechoic chamber using the same measurement devices as above, in this case with the single patch antenna as radiating element. The radiation characteristics, shown in Fig. 6(a)–(c), have been normalized to the maximal radiated power for the first mode, so that the radiated power of each mode may be compared to the others. At the first resonant mode (the length of the patch is about half the guided wave length of the substrate), the pattern of the patch antenna has a single and very broad lobe with the main radiation direction being normal to the patch surface [Fig. 6(a)]. At the second mode (the patch length is about one guided wave length), the radiation pattern has two lobes with a zero in a direction normal to the patch surface [Fig. 6(b)] where previously the first mode showed a maximum. The third mode [Fig. 6(c)] has three lobes with one lobe in normal direction. This middle lobe is smaller than the other two lobes and about 15 dB weaker than the main lobe of the first mode [Fig. 6(a)]. When comparing these radiation characteristics with the reflection behavior of the PMC, the correspondence becomes apparent. At the first mode, the radiation of the patch array is in normal direction, hence, a strong resonance phenomenon is measurable. At the second mode, no radiation in normal direction exists. The third resonance shows a dip in the reflection coefficient, which amounts to about 15 dB for the patch array measurement.

Comparing the properties of a single patch and the ones of the patch array leads to the explanation of the functioning of the patch array as PMC. Outside the resonant frequencies of the patches, it reflects the power just like a PEC reflector. At the resonances of the patch, it first absorbs the energy from the incident wave, causes itself to resonate, and then reradiates the energy. The radiation pattern and the magnitude of the reflection coefficient are determined by the different modes of the patch [14].

For the present patch array, two properties have been shown, both by simulations and measurements: first, the reflection coefficient exhibits resonance phenomena that approximately correspond in their field distributions to resonances of a patch antenna. Second, at the resonances, the patch array shows reflection properties that are in analogy of PMC surfaces. We conclude that the patch array effectively acts as a PMC within a certain bandwidth whose width is to be determined. Therefore, it can be used as a reflector in an array antenna.

The bandwidth of PMC surfaces may be evaluated with two criteria. The first is a common criterion in literature that the phase should be $180° \pm 45°$. With this criterion, the patch array in Fig. 5 acts as a PMC in the frequency bands of 5.2 to 5.7 GHz (approximately 9.3%) and 17.4 to 17.5 GHz (approximately 0.6%). Another criterion is to evaluate the PMC surface mounted in a structure taking advantage of the functionality of the PMC surface.

In the patch array, the interpatch coupling arises at the gap discontinuity, but the patches operate in principle as a single patch, therefore, the main statements on the functioning of a single patch are also applicable to PMC surfaces. The first and most important result is that the resonant frequency depends on the size of each patch. Furthermore, when increasing the thickness of the supporting substrate, the bandwidth increases. The same holds if the permittivity of the substrate is decreased. Other statements are similarly applicable.

III. Parallel-Plate Modes Reduction by PMC Reflectors

The PMC surface is now used as a reflector for a large aperture coupled patch antenna array. Aperture coupled microstrip patch antennas are attractive candidates for many phased array applications because of their light weight, low profile, easy fabrication and high efficiency. They exhibit an excellent polarization purity, making them suitable for high resolution imaging radar systems [15]. Furthermore, by applying an amplitude taper over the array aperture, provided by a dedicated feed network, low sidelobe levels can be achieved.

On the backside of the array, a reflector shields the back-radiation to protect instruments on the backside of the antenna and increase the gain in the forward direction. Usually, a PEC reflector is used and placed at a $\lambda/4$ separation to the antenna to get a constructive radiation normal to the reflector.

The backside reflector and the slot layer build a parallel plate waveguide [16] with parallel-plate modes and surface waves being excited on both plates, which is a general phenomenon for aperture coupled antennas with reflectors. The parasitic radiation from the edges and the modified excitation of the slots caused by the parallel-plate modes and surface waves degrade the performance of the antenna.

To overcome the excitation of the parallel-plate modes, electromagnetic bandgap (EBG) substrates have been proposed for a single radiator [17]. There, by inserting periodic dielectric rods between the slot plate and the PEC reflector, the propagation of higher order modes is reduced, whereas the dominant mode (TM_0 mode) is unaffected. However, the inclusion of periodic dielectric rods into a patch antenna array is complicated and increases costs and weight.

Here, a different approach is proposed: the excitation of surface waves and parallel plate modes is reduced by utilizing a PMC reflector.

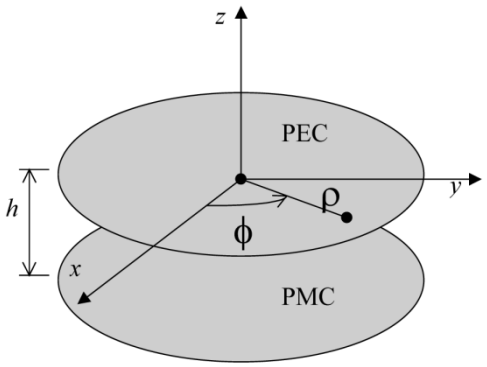

Fig. 7. Parallel plates: upper plate PEC; lower plate PMC.

A. Parallel Plate Mode Reduction

The parallel-plate modes with two PEC parallel plates are analyzed in [18]. In application here, the PMC reflector changes the boundary condition of the parallel plates and thus reduces the parallel-plate modes.

The structure considered consists of an upper PEC (slot layer), a dielectric separator and a lower artificial PMC (array reflector), as shown in Fig. 7.

For the TE^z modes, the E_ϕ component and H_ρ component are given by [18]

$$\begin{aligned} E_\phi(\rho,\phi,z) &= \frac{1}{\varepsilon}\frac{\partial F_z}{\partial \rho} \\ H_\rho(\rho,\phi,z) &= -j\frac{1}{\omega\mu\varepsilon}\frac{\partial^2 F_z}{\partial\rho\partial z} \end{aligned} \tag{9}$$

where the potential function F_z is

$$\begin{aligned} F_z(\rho,\phi,z) &= \left[C_1 H_m^{(1)}(\beta_\rho\rho) + D_1 H_m^{(2)}(\beta_\rho\rho)\right] \\ &\cdot[C_2\cos(m\phi)+D_2\sin(m\phi)][C_3\cos(\beta_z z)+D_3\sin(\beta_z z)] \end{aligned} \tag{10}$$

with

$$\beta_\rho^2 + \beta_z^2 = \beta^2. \tag{11}$$

In (10), $H_m^{(1)}(\beta_\rho\rho)$ and $H_m^{(2)}(\beta_\rho\rho)$ represent the Hankel functions of the first and the second kind, respectively. The coefficients $C_{1,2,3}$ and $D_{1,2,3}$ should be derived by the application of the appropriate boundary conditions.

The upper plate is a PEC, with the boundary conditions expressed in cylindrical coordinates

$$\begin{aligned} E_\rho(0\le\rho\le\infty, 0\le\phi\le 2\pi, z=0) &= 0 \\ E_\phi(0\le\rho\le\infty, 0\le\phi\le 2\pi, z=0) &= 0. \end{aligned} \tag{12}$$

The lower plate is a PMC and shows the following conditions

$$\begin{aligned} H_\rho(0\le\rho\le\infty, 0\le\phi\le 2\pi, z=-h) &= 0 \\ H_\phi(0\le\rho\le\infty, 0\le\phi\le 2\pi, z=-h) &= 0 \end{aligned} \tag{13}$$

where h is the separation between the two plates.

By inserting (9) and (10) to the boundary conditions (12) we get $\mathrm{C}_3 = 0$. To satisfy the conditions (13), the phase constant β_z should be:

$$\beta_z = \frac{\left(n+\frac{1}{2}\right)\pi}{h}\; n = 0,1,2,3,\ldots. \tag{14}$$

The cutoff is defined when $\beta\rho = 0$ in (11). Thus, the cutoff frequencies are obtained as follows:

$$(f_c)_n^{TE^z} = \frac{n+\frac{1}{2}}{2h\sqrt{\mu\varepsilon}}\; n = 0,1,2,3,\ldots \tag{15}$$

where μ and ε are the permeability and permittivity of the dielectric separator, respectively. For the TM^z mode, the same equation can be obtained. In contrast to a traditional parallel plate waveguide, which has a cutoff frequency at 0, the structure here has cutoff frequency $f_c > 0$. The cutoff frequencies of both the dominant TE and the dominant TM mode are the same and proportional to $1/h$. Therefore, if a PMC reflector is placed close enough to the slot plate so that the operating frequency of an antenna array is below the cutoff of the first TE and TM mode, no parallel-plate mode exists [19]. If the operation frequency of the antenna is f_0, the condition for a total suppression of parallel-plate modes is

$$h < \frac{1}{4f_0\sqrt{\mu\varepsilon}} \tag{16}$$

or in terms of wavelength, h should be smaller than a quarter of the guided wavelength of the medium between the plates.

In the following section, the described principle to suppress parallel plate waveguide modes is verified by measurements.

B. Measurements

For testing purposes, an 8×8 aperture coupled microstrip patch array has been designed. The antenna operates at 13.5 GHz and has a bandwidth of 7.4%. The array antenna configuration is itemized as follows:

- The patches for the antenna array are rectangular and have a size of $W_{\mathrm{rad}} = 10\ \mathrm{mm}$ and $L_{\mathrm{rad}} = 7.2\ \mathrm{mm}$.
- The patches are on a Rohacell substrate with $\varepsilon_{\mathrm{r,rad}} = 1.06$ and a thickness of $h_{\mathrm{rad}} = 1.2\ \mathrm{mm}$. On top of the radiating patches, a superstrate with $\varepsilon_{\mathrm{r,super}} = 2.32$ and $h_{\mathrm{super}} = 0.5\ \mathrm{mm}$ protects the radiating patches from environmental influences.
- The feed network is on a substrate with $\varepsilon_{\mathrm{r,feed}} = 2.32$ and $h_{\mathrm{feed}} = 0.5\ \mathrm{mm}$. The coupling slots have a size of $W_{\mathrm{slot}} = 5.6\ \mathrm{mm}$ and $L_{\mathrm{slot}} = 0.35\ \mathrm{mm}$.
- The distances between patches are 0.9 λ (wavelength of 13.5 GHz) and 0.75 λ in x and y directions, respectively. The complete array has a size of 165 mm $\times$ 145 mm, i.e., 7.4 $\lambda \times$ 6.5 λ.

The required sidelobe level is realized by an amplitude taper in the feed network with, in this case, a parabolic distribution on a pedestal. When multiplying the element pattern with the

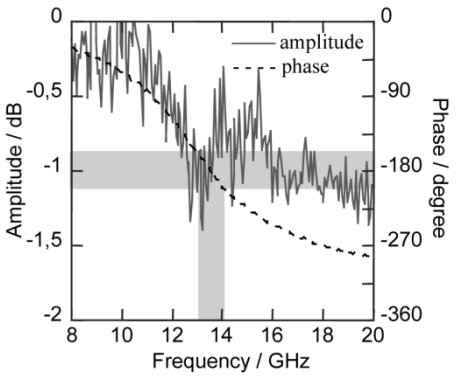

Fig. 8. Measured reflection properties of a PMC surface optimized for an operation from 13 to 14 GHz. Within the target bandwidth, the phase is $180° \pm 30°$.

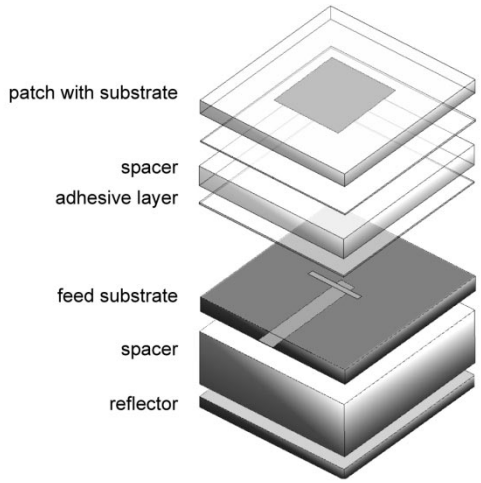

Fig. 9. Exploded view of a single element of the fabricated patch array antenna with reflector. On the backside of the superstrate, the radiating patches are located. The spacer ensures a correct distance between radiating element and coupling aperture. On the backside of the feed substrate, the feed network ensures the correct amplitude taper. The reflector finally is mounted on a second spacer.

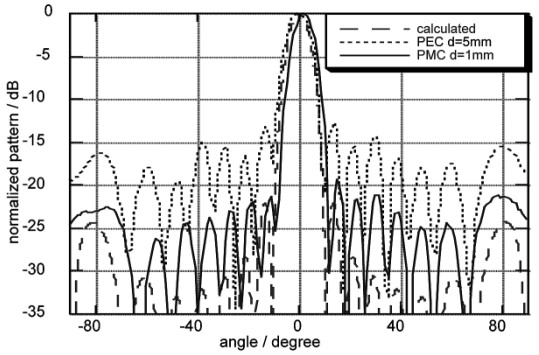

Fig. 10. E-plane radiation patterns at 13.5 GHz. The calculated curve shows the element pattern multiplied with the array factor, the PEC and PMC curves are actual measured values.

array factor, this gives a calculated sidelobe suppression better than -23 dB. This suppression can be used as reference for the realized antenna.

A PMC surface is designed for the center frequency of the array. As substrate, RT Duroid 5880 with a thickness of $h = 1.57$ mm and a relative permittivity of $\varepsilon_r = 2.2$ has been chosen to obtain a sufficient bandwidth. By estimating the size of the patches by (5) and by the initial process outlined earlier, a starting value for a numerical optimization procedure is obtained to be $L = W = 4.75$ mm and $s = 0.37$ mm (value that has been chosen for starting the design). The subsequent empiric optimization process is based on the experience with the optimization of patch antennas. During the process, the length L and the width W of the patches are modified simultaneously in order to obtain the correct resonant frequency at 13.5 GHz. With modifying the inter-patch distance s, the correct bandwidth is obtained. This process results in a patch size for the PMC surface of $W \times L = 3.43\,\text{mm} \times 3.43\,\text{mm}$, gap $s = 0.37$ mm, and a period of 3.8 mm. The measured reflection properties of the resulting PMC surface are shown in Fig. 8. Within the target bandwidth from 13 to 14 GHz the phase is 180° with a maximum variation of $\pm 30°$, the amplitude of the reflection coefficient is smaller than 1.5 dB. Hence, the structure is useable as PMC surface in the frequency band.

The antenna array with the exploded view of a single constituent element shown in Fig. 9 has been measured in the E plane in three configurations:

1) A PEC plate is used as a reflector and placed at a distance of $d = 5$ mm to the feed lines. The dielectric spacer is a 5-mm-thick Rohacell with $\varepsilon_r = 1.06$, the electrical distance between the feed lines and the spacer is then a quarter wavelength at 14.4 GHz. The quarter wavelength phase difference between 14.4 and 13.5 GHz is only 0.4 mm or 16°, which cannot account to a serious degradation of the PEC reflector at the target frequency of 13.5 GHz.
2) The PMC surface described above is used as a reflector. In theory, the distance d between PMC and feed lines should be zero, which is electrically not possible. At the same time, d needs to satisfy (16). Therefore, the PMC surface and the feed lines are chosen to be separated by a $d = 1$ mm Rohacell layer. This distance ensures that no parallel plate waveguide mode exists, since the resulting cutoff frequency from (16) is 73 GHz.
3) As reference, the copolarized pattern without reflector has been measured.

At $f = 13.5$ GHz, the normalized E-plane radiation patterns are shown in Fig. 10. The theoretical sidelobe suppression, again calculated by multiplying the element pattern with the array factor with the appropriate amplitude taper, for the array without reflector is $D_{\text{SL,theory}} < -23$ dB. In practice, the measured suppression is $D_{\text{SL,no-ref}} < -18.1$ dB. It worsens to $D_{\text{SL,PEC}} < -12.8$ dB when using a PEC reflector. The PMC reflector increases the sidelobe suppression to $D_{\text{SL,PMC}} < -20$ dB. At other frequencies in the operating band, similar improvements are achieved as reported in Table I. The PMC reflector shows a higher sidelobe suppression than both the antenna with no reflector by about 2 dB and the antenna with PEC reflector by about 6 dB.

An improvement of the sidelobe level compared to PEC backed array antennas should always be experienced when

TABLE I
MEASURED SIDELOBE SUPPRESSION FOR AN 8×8 APERTURE COUPLED MICROSTRIP PATCH ARRAY WITHOUT REFLECTOR, WITH A PEC REFLECTOR, AND WITH A PMC REFLECTOR. (SIZES ARE GIVEN IN THE TEXT)

reflector type	frequency		
	13 GHz	13.5 GHz	14 GHz
without reflector	-18.2 dB	-18.1 dB	-18.0dB
with PEC reflector	-13.0 dB	-12.8 dB	-13.1 dB
with PMC reflector	-19.1 dB	-20.0 dB	-16.0 dB

using PMC reflectors. The actual height of the sidelobes is caused by the feeding coefficients of each antenna array element. If the coefficients are modified by parasitic coupling, parallel plate modes or reflection phenomena, the sidelobe level is increased considerably. Suppressing the parallel plate modes is, hence, an efficient means to improve sidelobe level compared to PEC-backed antennas.

In the band, the best sidelobe suppression with a PMC is $D_{\mathrm{SL,PMC}} < -30\ \mathrm{dB}$, measured at 13.25 GHz. Due to the additional phase delay caused by the 1 mm separation of the PMC with the feed lines, the center frequency for an in-phase reflection has been shifted downward. Designing a PMC for a slightly higher center frequency can compensate this effect.

IV. CONCLUSION

A patch array consisting of square patches has been developed and its PMC properties at certain frequencies have been verified by measurements. The relation between the PMC patch array and a single patch antenna has been investigated. The structure has been described using an equivalent transmission line circuit, which includes the contributions of the patches, the substrate, and the intermediate gaps. The circuit model allows to design simple PMC surfaces. By comparing the reflection properties of the PMC with the radiation pattern of patches, a novel explanation for the functioning of the PMC surface is given.

PMC surfaces can be used as reflectors, e.g., in aperture coupled patch array antennas, to suppress parallel plate waveguide modes. Additionally, PMC surfaces can be placed with a smaller separation to the feed lines of the patch array compared to a PEC reflector. Thus, the antenna array has a smaller profile and is potentially lighter. For the presented test case, the PMC surface shows a 6 dB higher sidelobe suppression than with a PEC reflector, and still 1 to 2 dB than with no reflector.

REFERENCES

[1] D. Sievenpiper, L. Zhang, R. Broas, N. G. Alexopolous, and E. Yablonovitch, "High-impedance electromagnetic surfaces with a forbidden frequency band," *IEEE Trans. Microwave Theory Tech.*, vol. 47, pp. 2059–2074, Nov. 1999.

[2] K.-P. Ma, K. Hirose, F.-R. Yang, Y. Qian, and T. Itoh, "Realization of magnetic conducting surface using novel photonic bandgap structure," *Electron. Lett.*, vol. 34, no. 21, pp. 2041–2042, Oct. 1998.

[3] F.-R. Yang, K.-P. Ma, Y. Qian, and T. Itoh, "A novel TEM waveguide using uniplanar compact photonic-bandgap (UC-PBG) structure," *IEEE Trans. Microwave Theory Tech.*, vol. 47, pp. 2092–2098, Nov. 1999.

[4] W. Yu, D. H. Werner, and R. Mittra, "Reflection characteristic analysis of an artificially synthesized absorbing medium," *IEEE Trans. Magn.*, vol. 37, pp. 3798–3802, Sept. 2001.

[5] J. Haala, Y. Zhang, J. von Hagen, and W. Wiesbeck, "Band-selective extraction of resonant frequencies in high-Q resonators," *Microwave Opt. Technol. Lett.*, vol. 29, no. 6, pp. 438–441, June 2001.

[6] Y. Zhang, J. von Hagen, and W. Wiesbeck, "Patch array as artificial magnetic conductors for antenna gain improvement," *Microwave Opt. Technol. Lett.*, vol. 35, pp. 172–175, Nov. 2002.

[7] H. Pues and A. Van de Capelle, "Accurate transmission-line model for the rectangular microstrip antenna," *Proc. Inst. Elect. Eng.*, pt. H, vol. 131, pp. 334–340, Dec. 1984.

[8] A. G. Derneryd, "Linearly polarized microstrip antennas," *IEEE Trans. Antennas Propagat.*, vol. AP-24, pp. 846–851, Nov. 1976.

[9] L. I. Basilio, J. T. Williams, and D. R. Jackson, "The characterization of a slot discontinuity between two microstrip patch conductors," in *Proc. ICEAA'01*, Torino, Italy, 2001, pp. 251–254.

[10] K. C. Gupta, R. Garg, I. Bahl, and P. Bhartia, *Microstrip Lines and Slotlines*. Norwood, MA: Artech House, 1996.

[11] N. G. Alexopoulos and S.-C. Wu, "Frequency-independent equivalent circuit model for microstrip open-end and gap discontinuities," *IEEE Trans. Microwave Theory Tech.*, vol. 42, pp. 1268–1272, July 1994.

[12] C. Balanis, *Antenna Theory, Analysis, and Design*, 2nd ed. New York: Wiley, 1997.

[13] J. J. Lee and R. J. Broas, "Back-scatter measurements of Hi-Z ground plane," in *Proc. IEEE Int. Symp. Antennas Propagation AP-S'02*, June 2002, pp. 760–763.

[14] Y. Zhang, J. v. Hagen, E. Gschwendtner, and W. Wiesbeck, "Finite patch array as reflector for antenna gain improvement and size reduction," in Proc. URSI, Maastricht, The Netherlands, Aug. 2002.

[15] F. Rostan and W. Wiesbeck, "Aperture-coupled microstrip patch arrays for future spaceborne polarimetric SAR systems," in *Proc. Eur. Conf. Synthetic Aperture Radar EUSAR'1996*, Königswinter, Germany, Mar. 1996, pp. 209–212.

[16] H. Lentz, H. Braun, M. Younis, C. Fischer, W. Wiesbeck, and C. Mavrocordatos, "Concept and realization of an airborne SAR/interferometric radar altimeter system (ASIRAS)," presented at the Geoscience and Remote Sensing Symp., IGARSS' 2002, Toronto, ON, Canada, June 2002.

[17] J. D. Shumpert, W. J. Chappell, and L. P. B. Katehi, "Parallel-plate mode reduction in conductor-backed slots using electromagnetic bandgap (EBG) substrates," *IEEE Trans. Microwave Theory Tech.*, vol. 47, pp. 2099–2104, Nov. 1999.

[18] C. Balanis, *Advanced Engineering Electromgnetics*. New York: Wiley, 1989.

[19] Y. Zhang, M. Younis, C. Fischer, J. v. Hagen, and W. Wiesbeck, "Periodic patch array as reflector for low sideloble levels in arrays," presented at the 12e Journees Int. De Nice Sur Les Antennes Jina', Nice, France, Nov. 2002.

Ying Zhang (S'90) received the B.S. and M.S. degrees from the Jiaotong University Xi'an, China, in 1989 and 1992, respectively.

From 1992 to 1996, she was a lecturer with Zhejiang University, China. From 1999 to 2002, she was with the Institut für Höchstfrequenztechnik and Elektronik (IHE), Universität Karlsruhe (TH), Germany, as a Research Assistant. Her research interests during this period included broad-band conformal antennas, numerical calculations of electromagnetic fields, and microwave processing. Since September 2002, she has been with Hirschmann Electronics GmbH & Company KG, Germany, engaged in car communication systems, especially integrated car antenna system design.

Jürgen von Hagen (S'97–M'98–SM'02) received the M.S.E.E. (Dipl.-Ing.) and the Ph.D.E.E. (Dr.-Ing.) degrees from the Universität Karlsruhe (TH), Germany, in 1994 and 1997, respectively, and the Venia Legendi, also from the Universiät Karlsruhe (TH), in applied electromagnetic field theory in 2002.

From 1994 to 1997, he was with the Comité National de la Recherche Scientifique (CNRS), France, working on electromagnetic compatibility. In 1998, he held a Postdoctoral position with the Electromagnetics Research Laboratory, Pennsylvania State University, State College. From 1999 to 2002, he was with the Institut für Höchstfrequenztechnik und Elektronik (IHE), Universität Karlsruhe (TH), where he fulfilled the positions of Lecturer responsible for planar and conformal antennas, as well as numerical techniques in electromagnetics, and of Research Assistant for automotive communications and for industrial applications of microwaves, microwave heating processes, and EMC. Since 2002, he has been with the Development Department, Daimler-Chrysler AG, at the same time, he continues to teach courses on printed antennas and on electromagnetics at the Univerität Karlsruhe (TH). His research interests include electromagnetic theory, numerical techniques including frequency and time domain techniques, planar and conformal antennas, industrial applications of microwave power, and automotive communications and sensors.

Dr. von Hagen is Member of ACES and VDE.

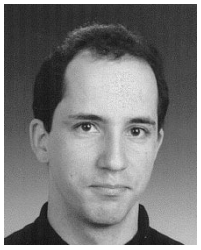

Marwan Younis (S'95) was born in Las Cruces, NM, in 1970. He received the B.E.E. degree from the College of Engineering, University of Baghdad, Iraq, in 1992, and the Dipl.-Ing. degree in electrical engineering from the Universität Karlsruhe (TH), Germany, in 1997, where he is currently working toward the Ph.D. (Dr.-Ing.) degree.

Since 1998, he has been a Research Scientist with the Institut für Höchstfrequenztechnik und Elektronik (IHE), Universität Karlsruhe (TH). His research fields include SAR systems, forward looking radar systems, microstrip antennas, and nonuniform antenna arrays. He serves as a lecturer for *Advanced Radio Communication* at the Universität Karlsruhe (TH).

Christian Fischer (S'98) was born in Karlsruhe, Germany, in 1970. He received the M.S.E.E. (Dipl.-Ing.) degree in electrical engineering from the Universität Karlsruhe (TH), Germany, in 1997, where he is currently working toward the Ph.D. (Dr.-Ing.) degree.

Since 1997 he has been a Research Assistant with the Institut für Höchstfrequenztechnik und Elektronik (IHE), Universität Karlsruhe (TH). His research topics include ground penetration radar measurements and imaging, antenna development and stochastic channel modeling. He serves as a lecturer on *Radar System Engineering* for the Carl Cranz Series for Scientific Education.

Werner Wiesbeck (SM'87–F'94) received the M.S.E.E. (Dipl.-Ing.) and Ph.D.E.E. (Dr.-Ing.) degrees from the Technical University of Munich, Munich, Germany, in 1969 and 1972, respectively.

From 1972 to 1983, he held various positions with AEG-Telefunken, including that of Head of Research and Development of the Microwave Division, Flensburg, Germany, and Marketing Director of the Receiver and Direction Finder Division, Ulm, Germany. During this time, he had product responsibility for millimeter-wave radars, receivers, direction finders, and electronic-warfare systems. Since 1983, he has been Director of the Institut für Höchstfrequenztechnik und Elektronik (IHE), Universität Karlsruhe (TH), Karlsruhe, Germany. His research interests include radar, remote sensing, wave propagation, and antennas. In 1989 and 1994, respectively, he spent a six-month sabbatical with the Jet Propulsion Laboratory, Pasadena, CA. He serves as a permanent Lecturer for *Radar System Engineering* and *Wave Propagation* for the Carl Cranz Series for Scientific Education.

Dr. Wiesbeck is a Member of an Advisory Committee of the European Union (EU) Joint Research Centre (Ispra/Italy). He was a Member of the IEEE Geoscience and Remote Sensing Society (IEEE GRS-S) Administrative Committee (AdCom) (1992–2000), Chairman of the IEEE GRS-S Awards Committee (1994–1998), Executive Vice President of the IEEE GRS-S (1998–1999), President of the IEEE GRS-S (2000–2001), Associate Editor of the IEEE TRANSACTIONS ON ANTENNAS AND PROPAGATION (1996–1999), and Past Treasurer of the IEEE German Section. He was General Chairman of the 1988 Heinrich Hertz Centennial Symposium and the 1993 Conference on Microwaves and Optics (MIOP'93). He has been a member of scientific committees of numerous conferences. He is an advisor to the German Research Council (DFG), the Federal German Ministry for Research (BMBF), and to industry in Germany.